DEUTSCHES ELEKTRONEN-SYNCHROTRON
Ein Forschungszentrum der Helmholtz-Gemeinschaft

DESY 21-094
arXiv:2106.09791
June 2021

TMD Parton Densities and Corresponding Parton Showers: The Advantage of Four- and Five-Flavour Schemes

H. Jung, S. Taheri Monfared

Deutsches Elektronen-Synchrotron DESY, Hamburg

ISSN 0418-9833

NOTKESTRASSE 85 - 22607 HAMBURG

To be sure that your reports and preprints are promptly included in the HEP literature database
send them to (if possible by air mail):

DESY Zentralbibliothek Notkestraße 85 22607 Hamburg Germany	DESY Bibliothek Platanenallee 6 15738 Zeuthen Germany

DESY 21-094
16 June 2021

TMD parton densities and corresponding parton showers: the advantage of four- and five-flavour schemes

H. Jung, S. Taheri Monfared

Deutsches Elektronen-Synchrotron DESY, Germany

Abstract

The calculations of $\mathrm{Z} + \mathrm{b\bar{b}}$ tagged jet production performed in the four- and five-flavour schemes allow for detailed comparison of the heavy flavour structure of collinear and transverse momentum dependent (TMD) parton distributions as well as for detailed investigations of heavy quarks radiated during the initial state parton shower cascade.

We have determined the first set of collinear and TMD parton distributions in the four-flavour scheme with NLO DGLAP splitting functions within the Parton-Branching (PB) approach. The four- and five-flavour PB-TMD distributions were used to calculate $\mathrm{Z} + \mathrm{b\bar{b}}$ tagged jet production at LHC energies and very good agreement with measurements obtained at $\sqrt{s} = 8, 13$ TeV by the CMS and ATLAS collaborations is observed.

The different configurations of the hard process in the four- and five-flavour schemes allow for a detailed investigation of the performance of heavy flavor collinear and TMD parton distributions and the corresponding initial TMD parton shower, giving confidence in the evolution of the PB-TMD parton densities as well as in the PB-TMD parton shower.

1 Introduction

Practical theoretical predictions for experimental measurements at high-energy hadron colliders require detailed simulations with the help of Monte Carlo event generators including parton showers and hadronization [1–5]. While significant progress has been achieved in the last decade on the simulation of processes by matching and merging methods [6–10] to combine next-to-leading order (NLO) matrix element calculations with parton showers, the parton shower is still treated separately from the parton densities. Only the Parton-Branching (PB) approach [11–13] with transverse momentum dependent (TMD) parton distributions allows a direct mapping of the parton shower to the TMD parton distribution. The CASCADE3 Monte Carlo event generator [5] uses PB-TMDs and simulates corresponding PB-TMD parton shower for initial state partons.

The description of the Drell-Yan (DY) transverse momentum spectrum at different center-of-mass energies $\sqrt{s}$ and for different DY masses m_{DY} applying PB-TMDs is very successful, as shown in detail in Refs. [11, 14, 15]. In this article we describe a detailed investigation of the corresponding PB-TMD parton shower by making use of Z production in association with b-flavored jets.

The production of b-flavor jets can be calculated in two different approaches: the four-flavor-variable-number (4FLVN) or five-flavor-variable-number (5FLVN) scheme. In the four flavor approach, the b-quark is only produced in the hard process, no b-quark is present in the parton density. In contrary, in the five-flavor approach, the b-quark is treated similarly as other light quarks, the mass is taken into account as a threshold, only for scales above m_{b} the b-quark is included. Correspondingly, the calculation of the hard process is different: in the four-flavor scheme, the heavy quark is treated massive, while in the five-flavor scheme, except the mass threshold, all quarks are treated similarly.

In Fig. 1 we show the lowest order process for Z+ b-jet production at LHC energies for the 4FLVN and 5FLVN schemes.

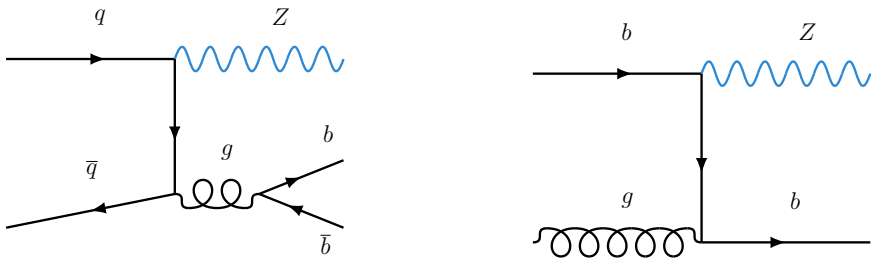

(a) $\mathrm{Z} + \mathrm{b\bar{b}}$ 4FLVN diagram (b) $\mathrm{Z} + \mathrm{b}$ 5FLVN diagram

Figure 1: Example of the lowest order diagrams for Z+b production in 4FLVN (a) and 5FLVN (b) schemes.

While the parton densities in the 4FLVN and 5FLVN schemes are different (and have to be determined separately), also the contribution from the parton shower is different: for $\mathrm{Z} + \mathrm{b\bar{b}}$ production at lowest order in the 4FLVN scheme the matrix element plays the dominant role, in the 5FLVN scheme the additional $\bar{\mathrm{b}}$-quark is contained in the parton density and is generated in the corresponding parton shower. Predictions obtained in the 4FLVN- and 5FLVN-schemes allow a comparison of the treatment b partons in collinear and TMD parton densities as well as in the corresponding initial state TMD parton shower.

This article is organised as follows: in Section 2 we describe the determination of the 4FLVN and 5FLVN TMD distributions applying the PB-method to fit inclusive HERA DIS measurements. In Section 3 we describe the calculation of Z+ b jet production at the LHC and compare predictions obtained in the 4FLVN and 5FLVN with measurements from CMS at $\sqrt{s} = 8$ TeV [16], discuss the role of the PB-TMD parton shower and show the consistency of the 4FLVN and 5FLVN approaches. In Section 4 we summarize our results.

2 PB-TMD parton densities in 4FLVN- and 5FLVN-schemes

The PB approach was developed in Ref. [12, 13] to solve the DGLAP [17–20] evolution equation and to calculate the TMD densities for all flavors over a large range in longitudinal momentum fraction x and the evolution scale μ^2. Collinear and TMD parton densities were ob-

tained in Ref. [11] using NLO DGLAP splitting functions, where the parameters of the initial starting distributions were obtained from a fit to inclusive DIS measurements at HERA [21]. Those parton distributions were obtained in the 5FLVN-scheme using a mass of the b-quark of $m_{\rm b} = 4.5$ GeV and a value for the strong coupling at five flavors of $\alpha_{\rm s}(m_{\rm Z}^{(5)}) = 0.118$.

In the PB approach the TMD evolution equations are written as:

$$\mathcal{A}_a(x,k_{\rm T}^2,\mu^2) = \Delta_a(\mu^2)\,\mathcal{A}_a(x,k_{\rm T}^2,\mu_0^2) + \sum_b \int \frac{dq'^2}{q'^2}\,\frac{d\phi}{2\pi}\frac{\Delta_a(\mu^2)}{\Delta_a(q'^2)}\,\Theta(\mu^2-q'^2)\,\Theta(q'^2-\mu_0^2)\,\times \int_x^{z_M}\frac{dz}{z}\,P_{ab}^{(R)}(\alpha_{\rm s},z)\,\mathcal{A}_b\left(\frac{x}{z},k_{\rm T}'^2,q'^2\right)\ , \quad (1)$$

where $\mathcal{A}_a(x,k_{\rm T}^2,\mu^2)$ is the probability distribution for flavour a carrying the longitudinal momentum fraction x of the hadron's momentum and transverse momentum $k_{\rm T}^2$ at the evolution scale μ^2; z and q'^2 are the branching variables, with z being the longitudinal momentum transfer at the branching, and q'^2 the momentum scale at which the branching occurs; $k'_{\rm T} = |\mathbf{k} + (1-z)\mathbf{q}'|$ is the rescaled transverse momentum of the emitted parton; ϕ is the azimuthal angle between $\mathbf{q}'$ and $\mathbf{k}$; μ_0 is the initial evolution scale; Δ_a is the Sudakov form factor; $P_{ab}^{(R)}$ are the real emission DGLAP splitting kernels.

Since the momenta $\mathbf{q} = \mathbf{q}'(1-z)$ of the emitted partons are treated explicitly, color coherence effects can be imposed by using angular ordering conditions, motivating to use the transverse momentum $q_{\rm T} = \sqrt{\mathbf{q}^2} = \sqrt{\mathbf{q}'^2(1-z)^2}$ as a scale choice for $\alpha_{\rm s}$; this condition was already applied in the PB-NLO-2018 Set 2 parton distributions described in Ref. [11], which is the distribution in the 5FLVN-scheme.

2.1 4FLVN scheme parton distributions

In the 4FLVN scheme, the b-quark does not appear as an active flavor in the parton evolution (practically we send $m_{\rm b} \to \infty$)). However, care has to be taken for the value of $\alpha_{\rm s}(m_{\rm Z})$, we use $\alpha_{\rm s}(m_{\rm Z}^{(4)}) = 0.1128$ as the four-flavor $\alpha_{\rm s}$, by a prescription motivated in Ref. [22].

The functional form of the starting distribution is the same as for the 5FLVN parton distributions in Ref. [11], however the parameters of the starting distribution are re-fitted to inclusive DIS measurements from HERA [21] (the same data set as used for 5FLVN parton distributions), yielding a $\chi^2/dof = 1.254$, very close to the one obtained for the 5FLVN-fit (using the `xFitter` package [23]). The uncertainties of the parton distributions coming from the experimental uncertainties of the data used are obtained with the Hessian method, as described in Ref. [11]. The model uncertainties are evaluated separately by varying the values of μ_0, q_{cut} and $m_{\rm c}$ around their default value as described in Ref. [11].

In Fig. 2 the 4FLVN and 5FLVN collinear parton densities are shown as a function of x at the evolution scale of $\mu = 100$ GeV.

Since there are less active flavors in the 4FLVN-scheme, the parton density distributions are slightly higher, which is especially visible in the gluon distribution.

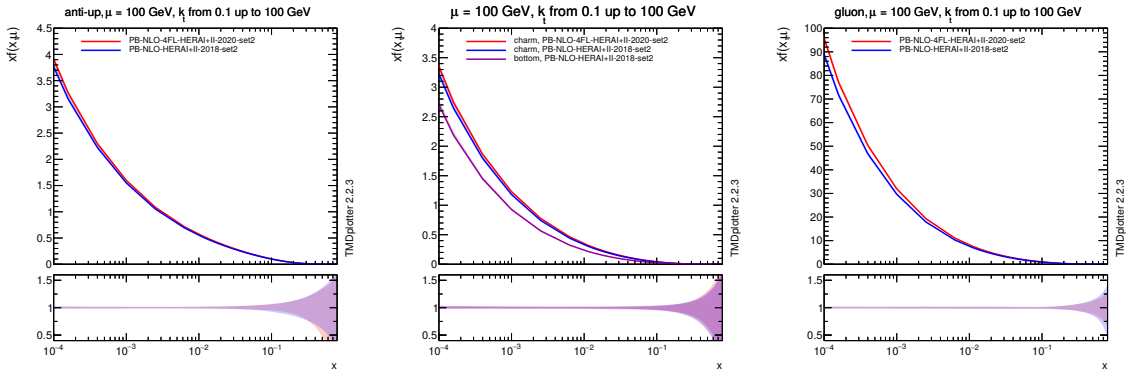

(a) $\bar{u}$ (b) charm and bottom (c) gluon

Figure 2: The $\bar{u}$ (a), charm and bottom (b) and gluon (c) 4FLVN and 5FLVN collinear parton densities for $\mu = 100$ GeV.

In Fig. 3 the parton distributions as a function of the transverse momentum k_{T} obtained in the 4FLVN and 5FLVN scheme for $\bar{\mathrm{u}}$, c, b and g densities at $x = 0.01$ and $\mu = 100$ GeV (typical values for Z production at the LHC) are shown. The b-quark exists only in the 5FLVN scheme, as shown in Figs. 2 and Fig. 3. At small k_{T} essentially the first term in Eq.(1) contributes, and the distributions are slightly different because of different magnitudes of the 4FLVN and 5FLVN distributions. At large k_{T} several branchings may have occurred and the differences between the distributions are washed out.

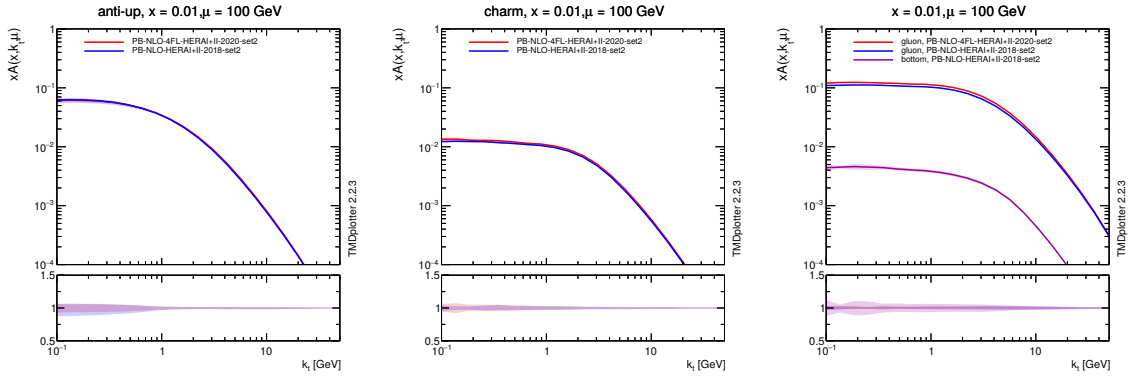

(a) $\bar{u}$ (b) charm (c) bottom and gluon

Figure 3: The $\bar{\mathrm{u}}$(a), charm (b), gluon and bottom (c) 4 flavour and 5 flavour TMDs as a function of k_t for $x = 0.01$ at $\mu = 100$ GeV.

In Fig. 2 and Fig. 3 the uncertainty band shown corresponds to the uncertainty obtained

from the experimental uncertainties, as well as the model uncertainties.

3 Z+ b-jet production

The diagrams contributing to Z+ b-jet production depend on the scheme used: in the 4FLVN-scheme, b-quarks are produced only in the hard matrix element, while in the 5FLVN- scheme, b-quarks are present already in the parton distribution and thus are treated similar to other lighter quarks. Examples of lowest order diagrams are shown in Fig. 1.

The hard processes are calculated at next-to-leading order (NLO) with the MADGRAPH5_AMC@NLO package (labelled as MCatNLO), as Z+ one parton process in the 5FLVN-scheme and $\mathrm{Z} + \mathrm{b\bar{b}}$ in the 4FLVN-scheme, using the corresponding 5FLVN or 4FLVN collinear parton densities with their different values of α_{s}. The renormalization and factorization scales are set to $\mu_R = \mu_F = 1/2 \sum_i H_{T,i}$ where i runs over all partons. The scale uncertainty is obtained by varying both scales independently by a factor 2 up and down. In the calculation of the hard process with the MC@NLO method [24–27], the HERWIG6 subtraction terms are applied, as they are relevant for the use with PB-TMDs and the PB-TMD parton shower implemented in CASCADE3 [5]. The transverse momenta of the incoming partons are obtained from the PB-TMDs, in the 5FLVN or 4FLVN-scheme, respectively.

Events are selected in the phase space of the CMS measurement [16] of a Z-boson in the presence of two b-tagged jets at $\sqrt{s} = 8$ TeV with $71 < m_{\mathrm{l\bar{l}}} < 111$ GeV, and the b-tagged jets obtained with the anti-k_{T} algorithm [28], with a distance parameter of $R = 0.5$ and with $p_{\mathrm{T}} > 30$ GeV and $|\eta| < 2.4$. In Fig.4 we show the transverse momentum of the Z-boson in the presence of two b-tagged jets at $\sqrt{s} = 8$ TeV obtained from calculations using the 4FLVN and 5FLVN-schemes with MCatNLO and PBTMDs and PBTMD parton shower.

In Fig. 4 also the predictions from parton level (LHE-level) are shown to illustrate the effect of the PB-TMD distribution on the transverse momentum spectrum of the Z-boson.

In Fig. 5 the cross section as a function of the azimuthal angular separation between the two b-tagged jets in $\mathrm{Z} + \mathrm{b\bar{b}}$ events is shown. In Fig. 5(a) the prediction coming from the 4FLVN calculation and in Fig. 5(b) the prediction using 5FLVN scheme is compared with the measurement. Also shown are the predictions coming from the pure partonic LHE level, indicating the role of PB-TMDs and PB-TMD shower. In the 4FLVN-calculation, the effect of inclusion of TMDs and TMD shower is small, since both b partons are already produced with NLO accuracy at the matrix element level, while in the 5FLVN-scheme, the effect of TMDs and parton shower is large, since a significant contribution comes from b-quarks inside the parton density and therefore must be simulated in the parton shower. The 4FLVN and 5FLVN calculations give very similar results and describe the measurements at a similar level, showing the consistency of both approaches.

3.1 The role of PB-TMD parton shower

In order to quantify the role of PB-TMD distributions and the corresponding parton shower on the differential cross section for $\mathrm{Z} + \mathrm{b\bar{b}}$ tagged jets as a function of azimuthal angular sep-

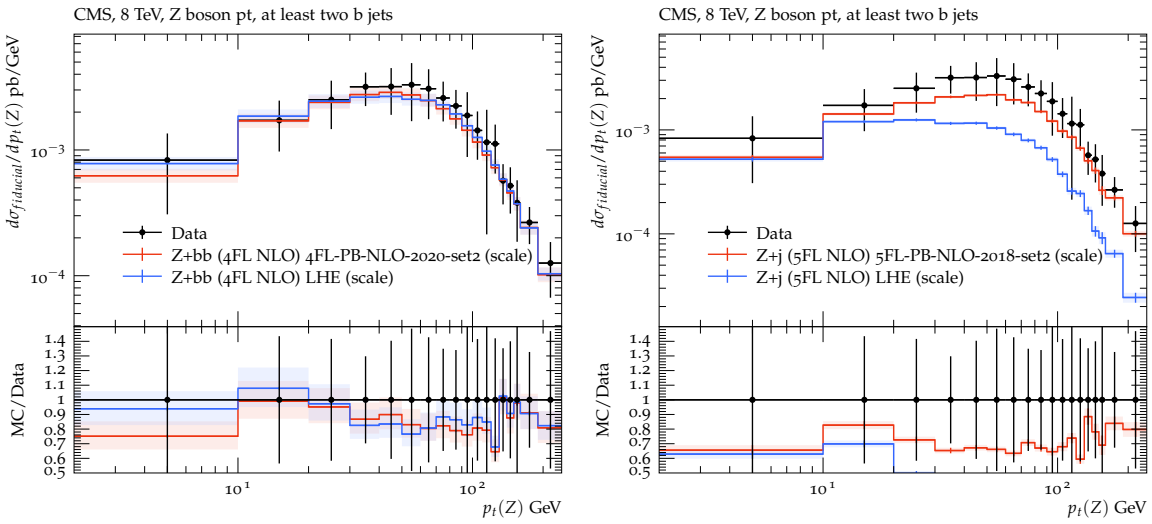

(a) (b)

Figure 4: Differential cross section for $\mathrm{Z} + \mathrm{b\bar{b}}$ tagged jets as a function of the transverse momentum of the Z-boson as measured by CMS [16] at $\sqrt{s} = 8$ TeV. The 4FLVN-prediction is shown in (a), the 5FLVN-prediction is shown in (b). In addition to the full prediction the result of using only the LHE files are shown.

aration $\Delta\phi_{\mathrm{b\bar{b}}}$, in Fig. 6 we show the breakdown of the different contributions, for the 4FLVN- and the 5FLVN calculations separately. One can clearly see, that the 4FLVN- calculation only weakly depends on PB-TMD and parton shower, while a very significant effect is observed for the 5FLVN- calculation.

In Fig. 7 we show a comparison of the full prediction obtained in the 4FLVN and 5FLVN-schemes and compared to a measurement by CMS [16] at $\sqrt{s} = 8$ TeV as well as to a measurement by ATLAS [29] at $\sqrt{s} = 13$ TeV, showing the very good consistency of both approaches, once the proper parton densities and the corresponding parton shower is included. Since the parton distributions are obtained from a fit to HERA data alone, no constraint comes from pp or $\mathrm{p\bar{p}}$ measurements. However in studies on inclusive jets it is observed that the PB-set2 yields predictions which are in general 10–20 % below the measurements. Taking a possible shift of 10–20 % into account, the Z+b measurements are very well described.

4 Conclusion

The calculations of $\mathrm{Z} + \mathrm{b\bar{b}}$ tagged jet production performed in the 4FLVN - and 5FLVN - schemes allow for detailed comparison of the heavy flavour structure of collinear and transverse momentum dependent (TMD) parton distributions as well as for detailed investigations of heavy quarks radiated during the initial state parton shower cascade.

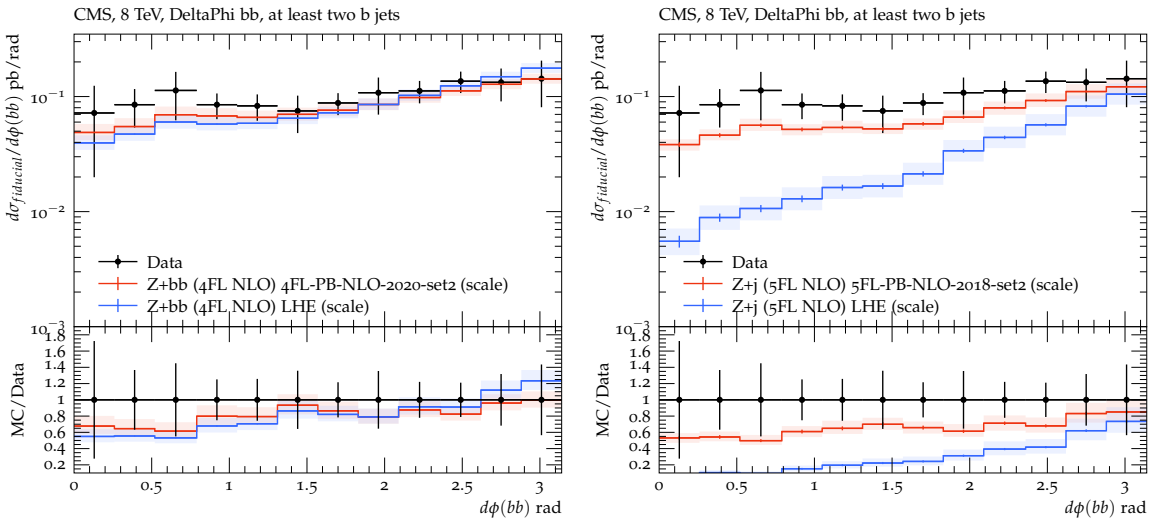

(a) (b)

Figure 5: Differential cross section for $\mathrm{Z} + \mathrm{b\bar{b}}$ tagged jets as a function of azimuthal angular separation $\Delta\phi_{\mathrm{b\bar{b}}}$ measured by CMS [16] at $\sqrt{s} = 8$ TeV together with predictions at parton level (LHE level) for subtraction terms and after inclusion of PB-TMDs and parton shower in 4FLVN (a) and 5FLVN (b) schemes.

We have determined the first set of collinear and TMD parton distributions in the 4FLVN-scheme with NLO DGLAP splitting functions within the PB approach. The functional form of the initial parton distributions follows the ones of the 5FLVN-scheme while the parameters are re-fitted to inclusive deep inelastic scattering measurements from HERA. The 4FLVN - and 5FLVN PB-TMD distributions were used to calculate $\mathrm{Z} + \mathrm{b\bar{b}}$ tagged jet production at LHC energies. The predictions obtained are in very good agreement with measurements obtained at $\sqrt{s} = 8, 13$ TeV by the CMS and ATLAS collaborations.

The different configurations of the hard process in the 4FLVN - and 5FLVN schemes allow for a detailed investigation of the performance of heavy flavor collinear and TMD parton distributions and the corresponding initial TMD parton shower. With consistently obtained 4FLVN - and 5FLVN PB-TMD distributions and TMD parton shower, very good agreement of the final cross sections between the two approaches is obtained, which gives confidence in the evolution of the PB-TMD parton densities as well as in the PB-TMD parton shower.

Acknowledgments.

We thank Sasha Zenaiev and Francesco Hautmann for many discussions. We are grateful for many discussions on Z+bproduction to S. Baranov, A. Lipatov and M. Malyshev. STM thanks the Humboldt Foundation for the Georg Forster research fellowship and gratefully

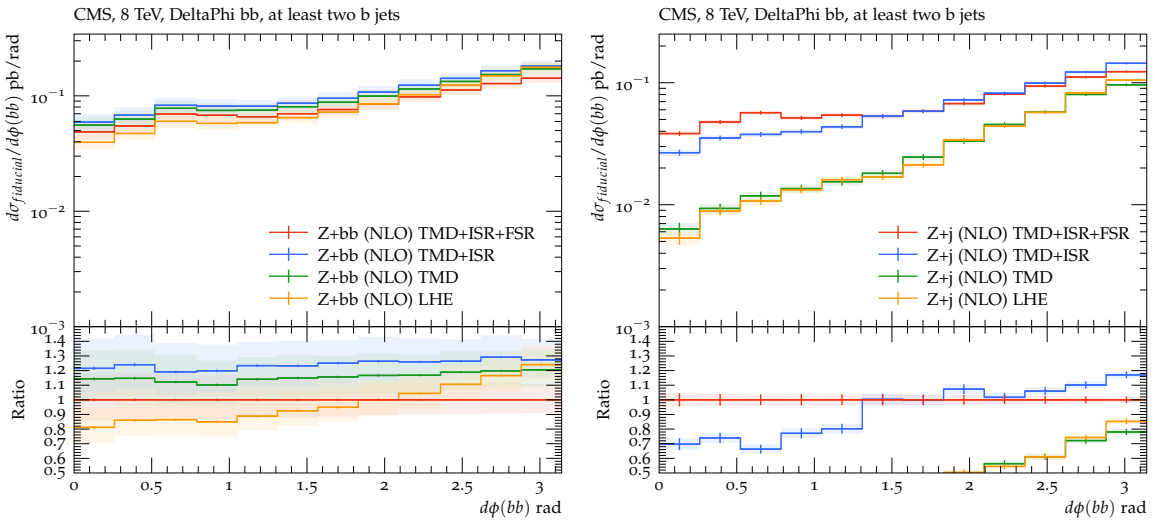

(a) (b)

Figure 6: Differential cross section for Z+b$\bar{\text{b}}$tagged jet production as a function of azimuthal angular separation $\Delta\phi_{\text{b}\bar{\text{b}}}$ at at parton level (LHE level), after inclusion of PB-TMDs, initial state parton shower and final state parton shower. In (a) is shown the prediction obtained within the 4FLVN-scheme, in (b) the prediction obtained in the 5FLVN-scheme.

acknowledges support from IPM.

References

[1] T. Sjöstrand et al., "An introduction to PYTHIA 8.2", *Comput. Phys. Commun.* **191** (2015) 159, arXiv:1410.3012.

[2] M. Bahr et al., "Herwig++: physics and manual", *Eur. Phys. J. C* **58** (2008) 639–707, arXiv:0803.0883.

[3] J. Bellm et al., "Herwig 7.0/Herwig++ 3.0 release note", *Eur. Phys. J. C* **76** (2016) 196, arXiv:1512.01178.

[4] Sherpa Collaboration, "Event Generation with Sherpa 2.2", *SciPost Phys.* **7** (2019), no. 3, 034, arXiv:1905.09127.

[5] S. Baranov et al., "CASCADE3 A Monte Carlo event generator based on TMDs", *Eur. Phys. J. C* **81** (2021) 425, arXiv:2101.10221.

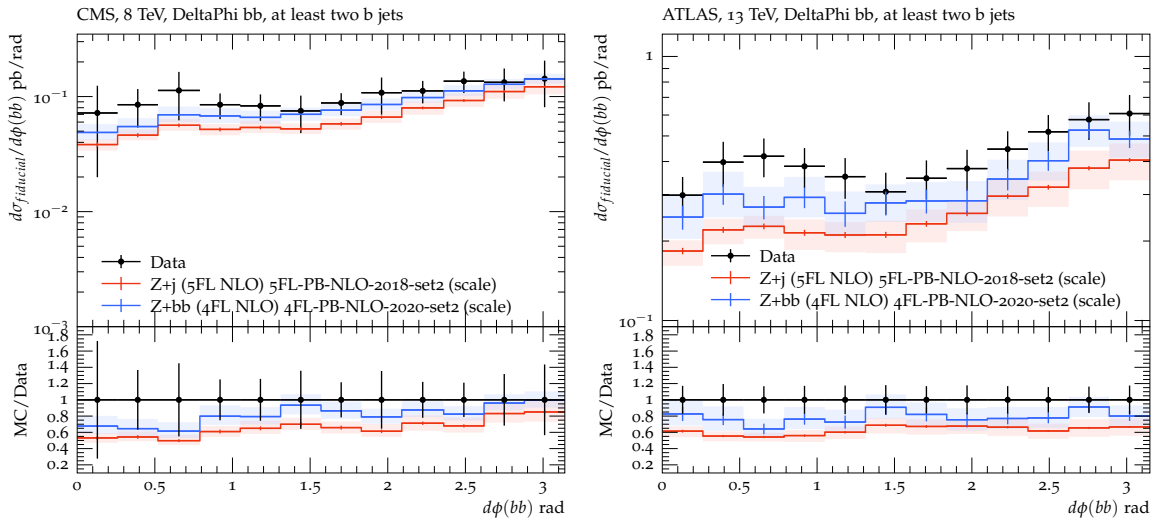

(a) (b)

Figure 7: Differential cross section for $\mathrm{Z} + \mathrm{b\bar{b}}$ tagged jet production as a function of $\Delta\phi_{bb}$ measured by CMS [16] at $\sqrt{s} = 8$ TeV (a) and at 13 TeV (b) as measured by ATLAS [29]. Shown are the predictions obtained in the 4FLVN- and 5FLVN- schemes.

[6] S. Frixione, P. Nason, and C. Oleari, "Matching NLO QCD computations with Parton Shower simulations: the POWHEG method", *JHEP* **0711** (2007) 070, arXiv:0709.2092.

[7] K. Hamilton, P. Nason, and G. Zanderighi, "MINLO: Multi-Scale Improved NLO", *JHEP* **10** (2012) 155, arXiv:1206.3572.

[8] S. Hoeche, F. Krauss, M. Schonherr, and F. Siegert, "A critical appraisal of NLO+PS matching methods", arXiv:1111.1220v1.

[9] J. Alwall et al., "The automated computation of tree-level and next-to-leading order differential cross sections, and their matching to parton shower simulations", *JHEP* **1407** (2014) 079, arXiv:1405.0301.

[10] R. Frederix and S. Frixione, "Merging meets matching in MC@NLO", *JHEP* **12** (2012) 061, arXiv:1209.6215.

[11] A. Bermudez Martinez et al., "Collinear and TMD parton densities from fits to precision DIS measurements in the parton branching method", *Phys. Rev. D* **99** (2019) 074008, arXiv:1804.11152.

[12] F. Hautmann et al., "Collinear and TMD quark and gluon densities from Parton Branching solution of QCD evolution equations", *JHEP* **01** (2018) 070, arXiv:1708.03279.

[13] F. Hautmann et al., "Soft-gluon resolution scale in QCD evolution equations", *Phys. Lett. B* **772** (2017) 446, arXiv:1704.01757.

[14] A. Bermudez Martinez et al., "The transverse momentum spectrum of low mass Drell–Yan production at next-to-leading order in the parton branching method", *Eur. Phys. J. C* **80** (2020) 598, arXiv:2001.06488.

[15] A. Bermudez Martinez et al., "Production of Z-bosons in the parton branching method", *Phys. Rev. D* **100** (2019) 074027, arXiv:1906.00919.

[16] CMS Collaboration, "Measurements of the associated production of a Z boson and b jets in pp collisions at $\sqrt{s} = 8$ TeV", *Eur. Phys. J. C* **77** (2017) 751, arXiv:1611.06507.

[17] V. N. Gribov and L. N. Lipatov, "Deep inelastic ep scattering in perturbation theory", *Sov. J. Nucl. Phys.* **15** (1972) 438–450. [Yad. Fiz.15,781(1972)].

[18] L. N. Lipatov, "The parton model and perturbation theory", *Sov. J. Nucl. Phys.* **20** (1975) 94–102. [Yad. Fiz.20,181(1974)].

[19] G. Altarelli and G. Parisi, "Asymptotic freedom in parton language", *Nucl. Phys. B* **126** (1977) 298.

[20] Y. L. Dokshitzer, "Calculation of the structure functions for Deep Inelastic Scattering and e^+e^- annihilation by perturbation theory in Quantum Chromodynamics.", *Sov. Phys. JETP* **46** (1977) 641–653. [Zh. Eksp. Teor. Fiz.73,1216(1977)].

[21] ZEUS, H1 Collaboration, "Combination of measurements of inclusive deep inelastic $e^{\pm}p$ scattering cross sections and QCD analysis of HERA data", *Eur. Phys. J. C* **75** (2015), no. 12, 580, arXiv:1506.06042.

[22] S. Dulat et al., "New parton distribution functions from a global analysis of quantum chromodynamics", *Phys. Rev. D* **93** (2016) 033006, arXiv:1506.07443.

[23] S. Alekhin et al., "HERAFitter", *Eur. Phys. J. C* **75** (2015) 304, arXiv:1410.4412.

[24] S. Frixione and B. R. Webber, "The MC@NLO 3.3 event generator", arXiv:hep-ph/0612272.

[25] S. Frixione, P. Nason, and B. R. Webber, "Matching NLO QCD and parton showers in heavy flavour production", *JHEP* **08** (2003) 007, arXiv:hep-ph/0305252.

[26] S. Frixione and B. R. Webber, "The MC@NLO event generator", arXiv:hep-ph/0207182.

[27] S. Frixione and B. R. Webber, "Matching NLO QCD computations and parton shower simulations", *JHEP* **06** (2002) 029, arXiv:hep-ph/0204244.

[28] M. Cacciari, G. P. Salam, and G. Soyez, "The anti-k_t jet clustering algorithm", *JHEP* **04** (2008) 063, arXiv:0802.1189.

[29] ATLAS Collaboration, "Measurements of the production cross-section for a Z boson in association with b-jets in proton-proton collisions at $\sqrt{s} = 13$ TeV with the ATLAS detector", *JHEP* **07** (2020) 044, arXiv:2003.11960.